JOURNAL OF AIRCRAFT
Vol. 35, No. 2, March–April 1998

Load Measurements on the Leading-Edge Extension, Wing, and Body of an F/A-18

B. H. K. Lee*
National Research Council, Ottawa, Ontario K1A OR6, Canada
and
S. Marineau-Mes†
University of Ottawa, Ottawa, Ontario K1N 6N5, Canada

The pressure difference across the wing and leading-edge extension (LEX) of a rigid 6% scale model of an F/A-18 was measured, and the integrated static and rms loads were computed. The total loads on the aircraft were obtained using a sting-mounted balance from which the body loads can be deduced by subtracting the LEX and wing loads. The effects of Mach number and angle of attack were analyzed and results for $M = 0.25$, 0.6, and 0.8 at $\alpha = 20$–35 deg are presented. The effectiveness of the LEX as a high-lift device is demonstrated by comparing the individual lift contributions from the wing and LEX at different angles of attack and Mach numbers. It is shown that the LEX vortex can generate large nonlinear static lift while inducing high unsteady lift on the aircraft.

Nomenclature

A_i = area of ith panel on wing surface
C_N = normal force coefficient
C'_N = rms value of normal force coefficient
c = wing mean aerodynamic chord, 0.21 m
M = freestream Mach number
N = normal force
p = unsteady pressure
p_{iL} = pressure on wing or LEX lower surface at ith panel
p_{iU} = pressure on wing or LEX upper surface at ith panel
q = dynamic pressure
Re_c = Reynolds number based on c
S_L = LEX surface area, 1.19×10^{-2} m^2
S_p = wing planform area, 1.34×10^{-1} m^2
S_W = wing surface area, 4.15×10^{-2} m^2
α = angle of attack

I. Introduction

THE International Follow On Structural Test Program (IFOSTP) is a joint Canadian and Australian venture to ensure the continued airworthiness of the CF/AF-18 under current operating conditions and to provide engineering data to allow for efficient life cycle management decisions. One of the primary objectives in this program is the collection of loads data for structural analyses. It was demonstrated from flight tests[1] that the flow past an F/A-18 wing at high angles of attack was very complex with large regions of separated flow on the wing upper surface. The ability of present computational fluid dynamics (CFD) codes to provide accurate load distributions at these flight conditions is doubtful.

To obtain static and dynamic loads on the wing and leading-edge extension (LEX) for selected critical maneuvers inside the flight envelope for IFOSTP, wind-tunnel tests were performed in the Institute for Aerospace Research (IAR) 1.5-m trisonic blowdown wind tunnel on a rigid 6% scale model of the F/A-18 instrumented with pressure transducers on the starboard wing and LEX. The results were also used to provide a better understanding of the flowfield past the F/A-18 wing, although the placing of the transducers in a relatively coarse grid was not ideal for this purpose. In Ref. 2, some preliminary results were presented from flow visualization studies and measurements of the unsteady pressure field. A more detailed study was presented in Ref. 3 where statistical results, such as power spectra, space-time cross-correlation and coherency of the pressure fluctuations were analyzed. Aside from the specific requirements for IFOSTP, the data collected from this series of tests are valuable to other programs at the IAR. For example, the steady-state results were used for computer-code validation while the unsteady results provide information on the dynamic load distributions that are necessary for wing buffeting and other dynamic response analyses.

It is common in fighter-type wing design to have high sweep angle and low aspect ratio. To provide the lift required for maneuvers at high angles of attack, a LEX is usually employed. The wings of an F/A-18 are typical of those found in most combat aircraft and an understanding of the flow past the wing is useful in any improvement to enhance the performance of the aircraft. The LEX on the F/A-18 has been quoted to contribute an excess of 22% of the total nonlinear lift at high incidences.[4]

This paper investigates the effects of Mach number and angle of attack on loads experienced by the F/A-18. The LEX and wing loads are computed from pressure measurements while those generated by the body are deduced from sting-balance measurements. Loads data for the LEX are presented to demonstrate its effectiveness as a high-lift device.

II. Wind-Tunnel Facility and Model

A. Wind-Tunnel Facility

The tests were performed in the trisonic blowdown wind tunnel at the IAR. The wind tunnel is a pressurized intermittent flow facility, and is capable of operating in the subsonic, transonic, and supersonic flow regimes. It has a Mach number range from $M = 0.1$ to 4.2. The walls of the 1.5×1.5 m transonic test section are perforated with 1.27-cm holes inclined 30 deg to the flow, thus allowing flow communication between the test section and a 3.65 m diameter by 4.87 m

Received Aug. 11, 1996; revision received Oct. 21, 1997; accepted for publication Oct. 21, 1997.

*Group Leader, Institute for Aerospace Research, Experimental Aerodynamics and Aeroelasticity; also Adjunct Professor, Department of Mechanical Engineering, University of Ottawa, Ottawa, Ontario, Canada. Associate Fellow AIAA.

†Graduate Student, Department of Mechanical Engineering.

length plenum chamber. The porosity of the walls is adjustable from 0.5 to 6%. For these tests, it was set at 4%. In subsonic and transonic tests, a hydraulically driven Mach number control system maintains the desired test section Mach number within ± 0.003 as the model pitches, and the stagnation pressure can be held constant to an accuracy of ± 137 Pa throughout the wind-tunnel run.

The test model was mounted on a cranked sting that forms part of the model support system. The strut can be programmed to move vertically and with the pitch linkage mechanism, the model angle of attack can vary from 0 to 33 deg. For high Mach number and dynamic pressure test conditions, aerodynamic loading causes bending of the sting that can increase the angle of attack by up to 2 deg.

B. Model

The model used in this study is a rigid 6% scale of the F/A-18, and a detailed description on the construction is given in Ref. 5. The center fuselage is bored to accept a 3.8-cm-diam Able Corp. sting balance. For these experiments, AIM-9 missiles were mounted on the wing tips and the leading- and trailing-edge flaps were set at 34 and 0 deg, respectively. The horizontal stabilator angle was set at -9 deg. These angles correspond to the F/A-18 auto flaps-up mode schedule settings at high angles of attack. Boundary-layer transition trips were installed on the wings, LEX, fins, stabilators, and forebody of the model.

The model starboard LEX and wing are instrumented with a total of 168 pressure transducers, 30 on the LEX and 138 on the wing. The position of these sensors is shown in Figs. 1 and 2, with an equal number on the upper and lower surface located directly opposite to each other. The transducers are semiconductor sensors (Kulite XCQ-062-50A) with an active diameter of 0.88 mm and a frequency response in excess of 50 kHz. They were flush mounted in pockets that were machined on the wing surfaces. Trenches were also machined on the wing surfaces to accommodate the electrical wirings. The pockets were filled with a silastomer after the sensors were mounted, and this served the purpose of protecting the transducers. The trenches were filled with an epoxy compound and hand-finished to the original wing profile. A detailed description of the calibration procedure and accuracy of the transducers is reported in Ref. 2.

The wind-tunnel data acquisition system consists of two separate subsystems: 1) a low-speed and 2) a high-speed data system. The low-speed system is used to control the tunnel operation, model positions, and record the wind-tunnel run conditions. These data are normally sampled at 100 Hz, and the computer used is a PDP 11/73. A micro-Vax-based high-speed data-acquisition system is available for collecting data at a high sampling rate for unsteady pressure measurements. The sampling frequency was set at 38.4 kHz in this wind-tunnel test and the data system is capable of collecting up to 10 million samples per second. The data are transferred at the end of the day to an 8-mm data cartridge. Data processing is performed on HP 9000/750 and IBM RS/6000 workstations.

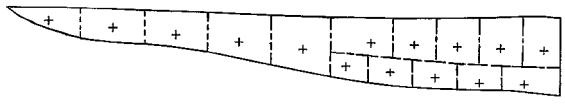

Fig. 1 Position of transducers and panels on LEX.

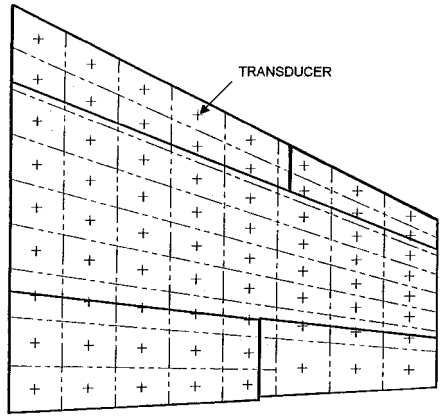

Fig. 2 Position of transducers and panels on wing.

III. Results and Discussion

A. Static Loads

To compute the steady and unsteady loads on the wing, the pressure difference across a transducer pair is formed from the time series, and C_{NW} is determined by the following equation:

$$C_{NW} = \sum_{i=1}^{69} (p_{iL} - p_{iU}) A_i / q S_W \tag{1}$$

The wing surface is divided into 69 panels, with each upper and lower transducer pair being in the middle of a panel and the pressure is assumed to be constant on each panel. The panel dimensions and locations on the wing are shown in Fig. 2. Because the leading-edge flaps are set at an angle relative to the plane of the wing, the projected area of the flaps onto the wing reference plane is used. For the LEX, C_{NL} is determined from Eq. (1) using 15 panels with dimensions shown in Fig. 1. The wing area S_W is replaced by S_L in Eq. (1).

Time-averaged normal force coefficients on the wing are shown in Fig. 3 for $M = 0.25$, 0.6, and 0.8 with α varying between 20 and 35 deg. Corresponding to these three Mach numbers, the values of q are 5.5, 26.8, and 39.9 kPa, respectively. The Reynolds numbers based on the wing mean aerodynamic chord are 1.60×10^6, 3.37×10^6, and 4.00×10^6, respectively. The effect of Mach number is small between the results at $M = 0.25$ and 0.8, whereas the curve for $M = 0.6$ shows higher normal force coefficients. The differences are not large and the small dependence on M could be attributed to the contributions to C_{NW} from the leading-edge vortices that are not strongly dependent on Mach number. Dividing C_{NW} by $(1 - M^2)^{1/2}$ shows the curves to be approximately evenly spaced with the $M = 0.6$ curve lying in the middle. The curves could not be collapsed using this compressibility factor.

It should be noted that the loads on the wing are influenced by the LEX, making it difficult to identify the wing-alone contribution to the combined loads. Ideally, the LEX should be removed, but this is not possible because the construction of the wind-tunnel model[5] is such that the LEX forms an integral part of the forebody section of the model.

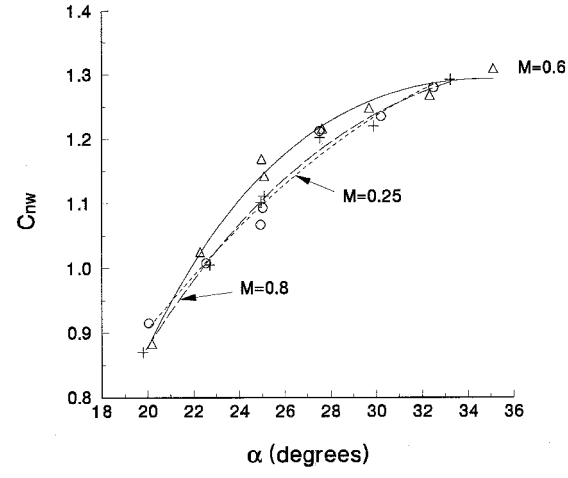

Fig. 3 Wing static normal force coefficient.

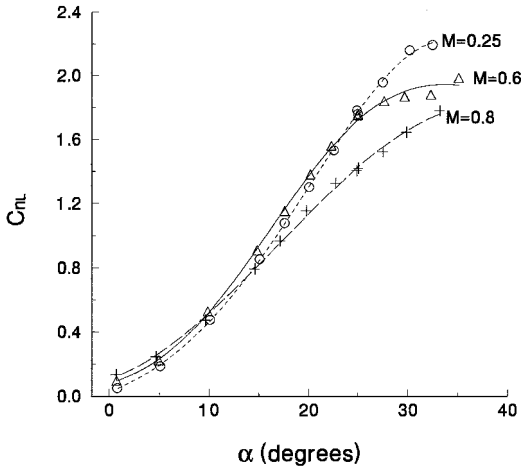

Fig. 4 LEX static normal force coefficient.

The static C_{NL} for the LEX is shown in Fig. 4 with α varying between 0 and 35 deg. The leading-edge flap angle was set at 34 deg in these tests and, at low angles of attack, this flap angle will not correspond to those programmed following the F/A-18 flap schedule. It is not known by what amount the flaps will affect the LEX pressure distributions at low α, although it is certain that the results will be influenced by the flap angles to some extent. The results shown in Fig. 4 for low α must, therefore, be interpreted with caution. They are included only to give an indication of the load variations with angle of attack. Figure 4 shows that on the LEX the $M = 0.25$ and 0.6 results are very close, except when α reaches 25 deg and beyond. The normal force coefficient at $M = 0.8$ is consistently below those for the other two lower M curves. For small α of less than 10 deg, the curves tend to coalesce. No detailed surface flow visualization studies such as those carried out in Ref. 6 have been performed for the various Mach numbers and the angle-of-attack range in the results presented in Fig. 4. Knowledge of the primary LEX vortices at these M and α will be useful to examine the behavior of C_{NL} with Mach number. However, the results from Fig. 4 indicate that the contribution of nonlinear lift caused by the LEX vortex is smaller at transonic Mach numbers.

The combined LEX and wing normal force coefficient is given in Fig. 5. It is seen that C_{NT} at $M = 0.8$ is lower than the curves for $M = 0.25$ and 0.6. The results are consistent from observation of the behavior of the individual C_{NW} and C_{NL} given in Figs. 3 and 4.

The total load on the aircraft measured from a sting balance is shown in Fig. 6, where C_{NB} is obtained using the wing planform reference area S_p. The effect of Mach number is also small, similar to the results shown for the wing. C_{NB} increases with M, that is, $(\partial C_{NB}/\partial M)_\alpha > 0$ for 20 deg < α < 35 deg, which is the range of α where measurements were taken. By comparison, Fig. 5 shows that $(\partial C_{NB}/\partial M)_\alpha < 0$ for α > 27 deg, and there exists a value of α between 20 and 27 deg, where $(\partial^2 C_{NB}/\partial M^2)_\alpha = 0$.

The LEX has been credited to contribute an excess of 22% of the static lift. It is not known how this number was determined by Frazier.[4] By coincidence, the ratio of the LEX to the combined area (wing and LEX) is approximately 0.22. It appears that this estimate may be obtained from area considerations only. Figures 3 and 4 show that the normal force coefficients on the LEX have values higher than those on the wing because the primary LEX vortex induces a low-pressure region on the LEX upper surface. The results for the normal force are given in Fig. 7, where the ratio of the force on the LEX to that on the wing is displayed as a function of α. This ratio depends on the Mach number and can reach much higher values than that quoted in Ref. 4. For example, at $M = 0.25$ and α = 33 deg, the LEX contributes to nearly 33% of the total lift.

Figure 8 shows the ratio of the loads on the LEX and wing as a percentage of the total loads measured from the sting balance. The LEX and wing area is only a fraction of the total aircraft projected area that generates the lift of the aircraft. The body contribution can be determined from the difference between the sting balance measurements and the loads computed from the pressure transducers. Figure 8 shows that a significant amount of lift is generated by the body. For example, at Mach

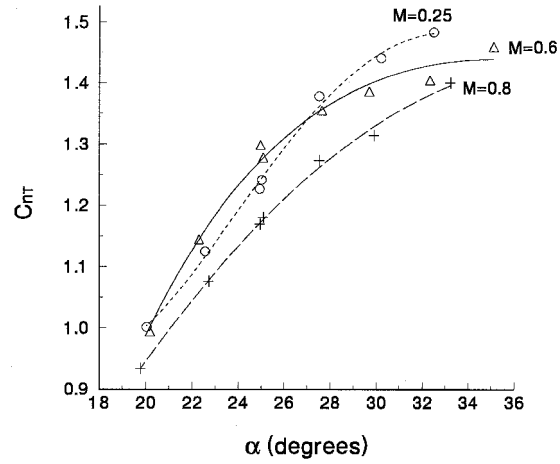

Fig. 5 Combined LEX and wing static normal force coefficient.

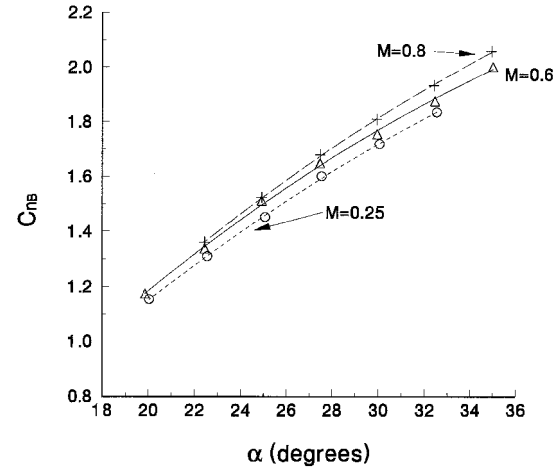

Fig. 6 Sting balance static normal force coefficient.

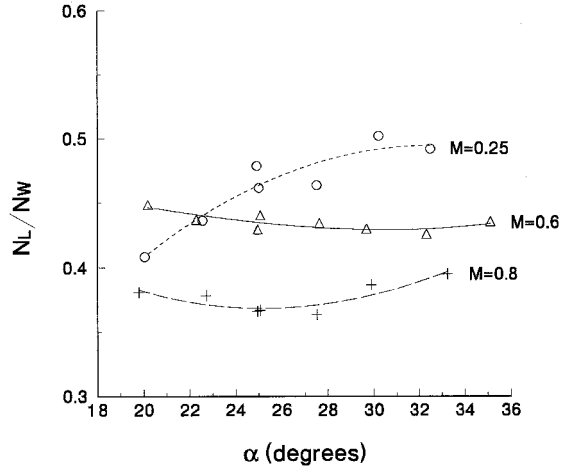

Fig. 7 Ratio of LEX/wing static normal force.

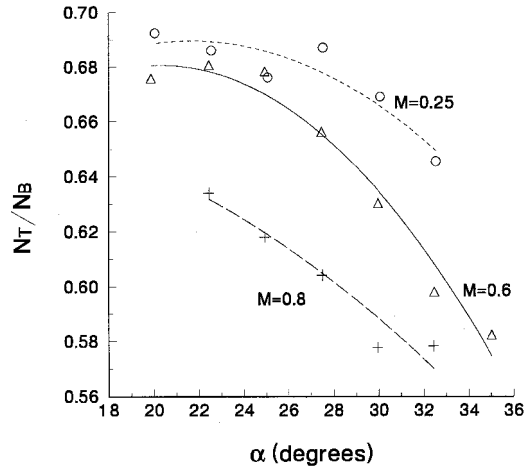

Fig. 8 Ratio of combined LEX and wing to balance static normal force.

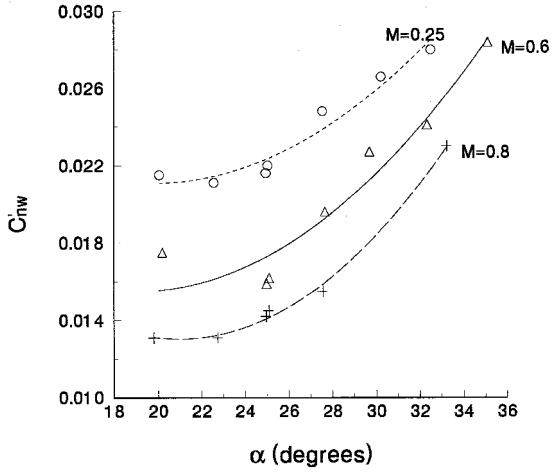

Fig. 9 RMS value of wing normal force coefficient.

number 0.6, the ratio N_T/N_B drops from approximately 68% at $\alpha = 20$ deg to 58% at $\alpha = 35$ deg. A decrease in N_T/N_B indicates the contribution of the body lift increases faster than that from the LEX and wing. The higher lift generated by the body at the larger angles of attack is a result of the stronger forebody and LEX vortices. Figure 8 also shows that the body contribution increases with Mach number, which is consistent with Figs. 5 and 6. For example, at $\alpha = 30$ deg, the body contributes approximately 33% of the total lift for $M = 0.25$, 37% for $M = 0.6$, and 42% for $M = 0.8$.

B. RMS Loads

Unsteady loads are computed using Eq. (1) and they are presented in this paper in the form of rms values. Figure 9 shows the variation of the rms load distributions on the wing with angle of attack for three Mach numbers. As expected, more severe separation at higher α accounts for the increase in C'_{Nw} with angle of attack. Both α and M affect the nature and size of the various separated flow regions. Compressibility effects are particularly important for $M \geq 0.8$ and they need to be examined in more detail from analyses of the surface pressure measurements. Surface flow visualization and off-body flow studies at various M and α are useful to further understand the complex flow separation phenomenon. Limited analyses on the unsteady pressure field at $M = 0.6$ and $\alpha = 30$ deg using statistical methods are reported in Ref. 7, which gave further insight in the observed behavior of the results.

The rms loads on the LEX given in Fig. 10 show small differences with Mach numbers up to $\alpha = 15$ deg. For the LEX, the effects of flap settings may not be sufficiently large to render the results shown in Fig. 10 totally invalid at values of α below 25 deg. The curve for $M = 0.25$ gives the largest C'_{NL} for α above 15 deg, up to the last data point at $\alpha = 33$ deg. The static C_{NL} does not show large differences from those at $M = 0.6$, and the higher fluctuations are unexplained and require off-body flow visualization to study the LEX vortex structure. This is similar for the wing where C'_{NW} is largest for $M = 0.25$ because the effect of the LEX vortex high-pressure fluctuations is felt downstream on the wing. The $M = 0.6$ and 0.8 results show a slowly varying trend between $\alpha = 15$ and 28 deg, and they collapse into a single curve for further increases in α. The behavior of the curve for $M = 0.25$ is different and the increase in the rms loads is approximately linear with α.

The total rms normal force coefficient is given in Fig. 11 and the shapes of the curves are similar to those for C'_{NW}. It is interesting to note that at a given Mach number, say, $M = 0.6$, the total rms loads can differ by a factor of 2 from $\alpha = 25$ to 35 deg.

Figure 12 shows the variations of C'_{NB} with α obtained from the sting balance. Results are given for two Mach numbers only because those for $M = 0.25$ were not recorded in the tests. The rms values from the balance are computed from analog signals averaged over 5–10 s. Similar to Figs. 11, Fig. 12 shows that unsteadiness expressed in coefficient form is larger at the lower Mach numbers.

The ratio of the rms loads on the LEX and wing as a function of α is given in Fig. 13. The characteristics of the curves for $M = 0.6$ and 0.8 is different from that at $M = 0.25$. This

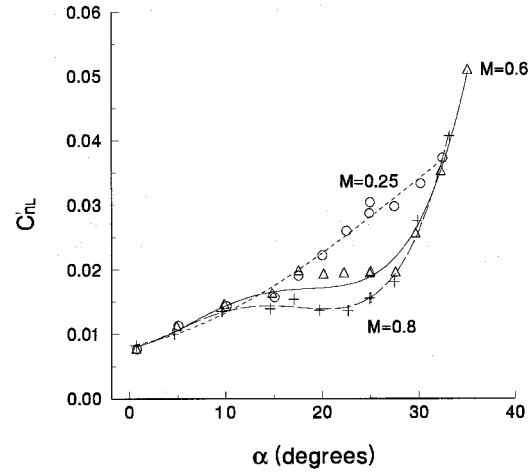

Fig. 10 RMS value of LEX normal force coefficient.

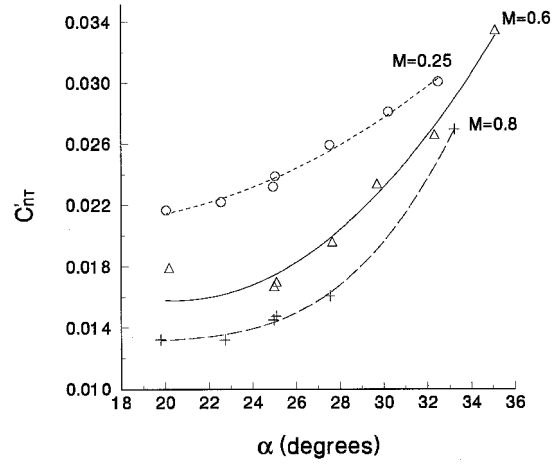

Fig. 11 RMS value of combined LEX and wing normal force coefficient.

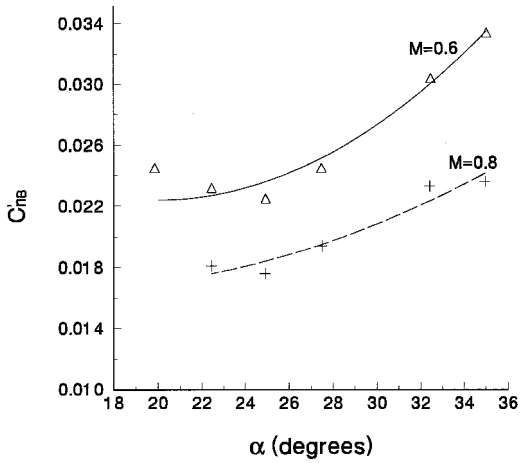

Fig. 12 RMS value of balance normal force coefficient.

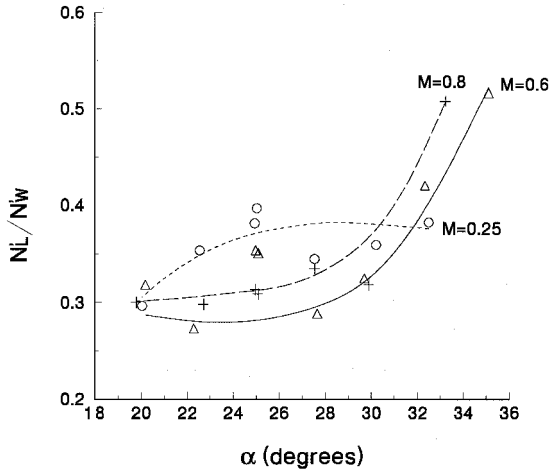

Fig. 13 Ratio of LEX/wing rms value of normal force.

can be deduced from the behavior of the rms normal force coefficient shown in Figs. 9 and 10. Although the LEX has approximately 28% of the wing's area for this particular flap setting, the rms value of the loads can be as high as 50% for $M = 0.6$ and 0.8 at α above 33 deg.

Figure 14 shows N'_T/N'_B plotted against α for $M = 0.6$ and 0.8. The contributions from the LEX and wing account for approximately 60% of the rms total load at $\alpha < 27$ deg. The Mach number effect is initially small and Fig. 14 shows that the combined LEX and wing generate larger unsteadiness with an increase in Mach number at angles of attack above a threshold value of 27 deg. The increase in unsteadiness with α can be attributed to the large separation regions on the wing upper surface found at the higher angles of attack.

The spacing of transducers used for load measurements is sufficient for the large attached flow region[1] on the inboard portion of the wing, which is under the influence of the LEX vortex system. On the inboard leading-edge flaps and near the the tip missiles, regions of flow separation and reattachment are observed and smaller panels for computing the loads are desired. However, the difficulties and expenses in mounting a large number of transducers on a small model precludes the addition of any more transducers than are already installed. Errors are introduced by assuming the pressure to be uniform across each panel, but from contour plots[2] of the steady and rms pressures, it is estimated that the errors may not be large for $\alpha < 35$ deg. A similar type of transducer spacing was used for load measurements on the vertical fins.[8] Results from pressure integration and strain gauges mounted on the fin root showed a maximum difference of approximately 10–15% for

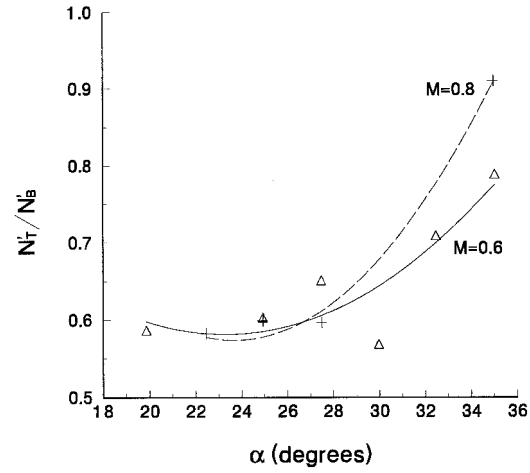

Fig. 14 Ratio of combined LEX and wing to balance rms value of normal force.

moderate to high α at M between 0.25 and 0.8. In the absence of any strain gauge measurements for the wing loads, it is difficult to estimate the error. However, from examining the spanwise and chordwise pressure distributions on both the wing and the vertical fin, it is safe to assume that the error is of the same order of magnitude in both cases.

Conclusions

The static and unsteady loads on the LEX and wing are successfully measured by computing time-averaged and rms values of the pressure transducer signals. The effects of Mach number and angle of attack were analyzed, and results for $M = 0.25$, 0.6, and 0.8 at $\alpha = 20$–35 deg are presented.

A large amount of nonlinear lift is generated by the body because of the presence of the forebody and LEX vortices, for example, at $M = 0.6$, the contribution of the body to the total loads changes with α from 32% at 20 deg to 42% at 35 deg. The unsteadiness at high angle of attack is largely generated by the LEX and wing.

From the behavior of the static and dynamic loads with α for the LEX and wing, a different trend is observed from the results at $M = 0.25$ compared with those at the higher values of $M = 0.6$ and 0.8. Further studies of the flow separation on the LEX and wing using surface flow visualization and off-body measurement techniques are required to understand the flow behavior with M and α. Detailed analysis of the surface pressure will provide some indication of the nature and intensity of the pressure fluctuations in the separated flow regions, but this requires a more closely spaced transducer grid to resolve the flow characteristics in some of the small separation regions.

The effectiveness of the LEX as a high-lift device is demonstrated by comparing the individual lift contributions from the wing and LEX at different angles of attack and Mach numbers. It is shown that the LEX vortex can generate large nonlinear static lift while at the same time induces very high unsteady lift on the aircraft.

Acknowledgments

The authors acknowledge the financial support from the Institute for Aerospace Research, the Department of National Defence, and the Natural Sciences and Engineering Research Council of Canada.

References

[1]Fisher, D. F., Del Frate, J. H., and Richwine, D. M., "In-Flight Flow Visualization Characteristics of the NASA F-18 High Alpha Research Vehicle at High Angles of Attack," NASA TM 4193, May 1990.

[2]Lee, B. H. K., Valerio, N. R., and Tang, F. C., "Steady and Unsteady Pressure Distributions on an F/A-18 Wing at α = 30 Deg," *Journal of Aircraft*, Vol. 31, No. 4, 1994, pp. 862–867.

[3]Lee, B. H. K., and Marineau-Mes, S., "Investigation of the Unsteady Pressure Fluctuations on an F/A-18 Wing at High Incidence," AIAA Paper 95-1865, June 1995.

[4]Frazier, F. A., "F-18 Hornet—LEX Fence Flight Test Results," Society of Experimental Test Pilots' Symposium, Beverly Hills, CA, Oct. 1988.

[5]Lee, B. H. K., and Brown, D., "Wind-Tunnel Studies of F/A-18 Tail Buffet," *Journal of Aircraft*, Vol. 29, No. 1, 1992, pp.146–152.

[6]Lee, B. H. K., and Valerio, N. R., "Vortical Flow Structure near the F/A-18 LEX at High Incidence," *Journal of Aircraft*, Vol. 31, No. 5, 1994, pp. 1221–1223.

[7]Lee, B. H. K., and Marineau-Mes, S., "Investigation of the Unsteady Pressure Fluctuations on an F/A-18 Wing at High Incidence," *Journal of Aircraft*, Vol. 33, No. 5, 1996, pp. 888–894.

[8]Lee, B. H. K., and Tang, F. C., "Unsteady Pressure and Load Measurements on an F/A-18 Vertical Fin," *Journal of Aircraft*, Vol. 30, No. 5, 1993, pp. 756–762.